NASA Technical Memorandum 104566, Volume 4

SeaWiFS Technical Report Series

Stanford B. Hooker, Editor
Goddard Space Flight Center
Greenbelt, Maryland

Elaine R. Firestone, Technical Editor
General Sciences Corporation
Laurel, Maryland

Volume 4, An Analysis of GAC Sampling Algorithms: A Case Study

Charles R. McClain
Goddard Space Flight Center
Greenbelt, Maryland

Eueng-nan Yeh and Gary Fu
General Sciences Corporation
Laurel, Maryland

National Aeronautics and
Space Administration

Goddard Space Flight Center
Greenbelt, Maryland 20771

1992

ABSTRACT

The Sea-viewing Wide Field-of-view Sensor (SeaWiFS) instrument will sample at approximately a 1 km resolution at nadir which will be broadcast for reception by realtime ground stations. However, the global data set will be comprised of coarser four kilometer data which will be recorded and broadcast to the SeaWiFS Project for processing. Several algorithms for degrading the one kilometer data to four kilometer data are examined using imagery from the Coastal Zone Color Scanner (CZCS) in an effort to determine which algorithm would best preserve the statistical characteristics of the derived products generated from the one kilometer data. Of the algorithms tested, subsampling based on a fixed pixel within a 4×4 pixel array is judged to yield the most consistent results when compared to the one kilometer data products.

1. INTRODUCTION

Early in the SeaWiFS design phase, questions arose regarding what the best scheme would be for producing reduced resolution global area coverage (GAC) data from the high resolution local area coverage (LAC) data generated by the scanner. The primary motivation for considering schemes other than a fixed pixel subsampling (a predefined element in a pixel array) was to maximize the number of cloud-free pixels. Other considerations included reduction of sensor noise (average-value techniques) and error introduced by high aerosol concentrations or clouds with low albedo (least-value techniques). A comprehensive study of GAC sampling techniques using Landsat and Advanced Very High Resolution Radiometer (AVHRR) data has been published by Justice et al. (1989) who found fixed pixel subsampling to be the best representation of the original full resolution data.

In this study, an analysis was performed on a single scene from the southeastern U.S. coast. The scene was selected because it encompasses both Case 1 and Case 2 waters (Morel and Prieur 1977). Of the five methods used in this study, the fixed pixel subsampling produced the best statistical fidelity to the LAC product. The other approaches can show significant deviations from the LAC statistical properties.

2. DATA PROCESSING

Various methods for reducing the resolution of an image were tested in order to compare their adequacy in retaining the statistical characteristics of the high resolution derived products. The SEAPAK (McClain et al. 1991) program L2GAC provides these methods as an option for the user while processing CZCS level-2 products. The GAC data analyses used in this study operate on 4×4 (pixel×line) blocks of data. L2GAC supports the AVHRR GAC generation scheme which operates on a 5×3 block of data, but it was not considered for this study. The level-2 products include the water-leaving radiances at 443, 520, and 550 nm; the aerosol radiance at 670 nm; the pigment concentration; and the Rayleigh radiance at 443 nm. L2GAC also allows the user to specify the atmospheric correction algorithm, the Ångström exponents, the ozone optical depths (default is computed from the Total Ozone Mapping Spectrometer (TOMS) Dobson Unit value at the center of the scene), the sensor calibration, the land/cloud threshold (750 nm), the haze threshold (670 nm), the water radiance scaling, and the water radiance product (upwelled subsurface water radiance or normalized water-leaving radiance). Ringing correction was not applied to the data (Mueller 1988).

L2GAC generates standard SEAPAK 512×512 pixel images by filling in the 4×4 pixel area with constant values. It is important to note that any pixel that fails either the land and cloud or haze threshold test is excluded from the analysis. In the case of fixed pixel subsampling where the pixel fails a threshold test, the entire 4×4 pixel area is assigned a grey level of either 0 (land) or 255 (cloud) to indicate an *invalid* pixel which is then excluded from the statistical analyses. The methods tested are described in Table 1, with the method numbering convention being the same as in the L2GAC program.

Table 1. GAC generation methods and the mechanisms used for each.

Method	Generation Mechanism
1	Average level-2 product (level-2 products are generated and then averaged).[1]
2	Fixed pixel subsampling (pixel [2,2] from the 4×4 array).
3	Mean radiance product (level-2 products are generated from mean radiances).
4	Lowest 670 nm radiance pixel.
5	NOAA/AVHRR subsampling which uses a 5×3 array of data.[2]
6	Lowest 750 nm radiance pixel.
7	Pigment concentration derived from mean L_W values as computed in Method 1.
8	Pigment concentration derived from mean Method 1 log(*concentration*) values.

1. Implemented only on the data processing system.
2. Not used in this study.

In the cases of average-value and least-value algorithms, the pixels that fail the flag criteria are ignored. The number of valid pixels within the 16 pixel array may be as few as one and the array will still be assigned a valid value. Thus, implementation of average-radiance-value (Method 3) and least-radiance-value (Methods 4 and 6) algorithms would require on-board processing for GAC data storage on the spacecraft. Methods 1, 7, and 8 can only be implemented on the ground.

To provide some background on the standard analysis methods (Gordon et al. 1983), the total radiance received by the CZCS is governed by the equation

$$L_t(\lambda) = t(\lambda)L_W(\lambda) + L_a(\lambda) + L_r(\lambda), \qquad (1)$$

where, λ is the wavelength, L_t is the total radiance, L_W is the water-leaving radiance, t is the diffuse transmittance of the atmosphere, L_a is the aerosol radiance, and L_r is the Rayleigh radiance. L_r depends upon the orientation between the sun, Earth, and satellite, and, for this analysis, $L_W(670)$ is assumed to be zero.

$L_a(\lambda)$ is related to $L_a(670)$ through an expression of the form

$$L_a(\lambda) \propto \left(\frac{\lambda}{670}\right)^{n(\lambda)} L_a(670), \qquad (2)$$

where, $n(\lambda)$ is the Ångström exponent. For the present analyses, the Ångström exponents were assumed to be 0. In this case, aerosol radiance equals $L_a(670)$ multiplied by a ratio of the solar constants times an exponential function of the solar and spacecraft zenith angles and the ozone optical thicknesses.

From the water-leaving radiances, pigment concentration is calculated using an equation of the form

$$[\text{chlorophyll } a + \text{phaeophytin}] = \alpha\left[\frac{L_W(\lambda)}{L_W(550)}\right]^{\beta}, \qquad (3)$$

where, pigment concentration is considered to be the sum of the concentrations of chlorophyll a and phaeophytin, α is a positive number, and β is negative.

A CZCS scene of the United States East Coast, covering the area approximately from 70–90°W and from 26–34°N, on October 28, 1979, was processed using L2GAC for this test. The full-resolution level-2 products were generated by another SEAPAK program, L2MULT. The inputs used in the level-2 processing are provided in Table 2. All wavelength dependent parameters in the table are given in order of increasing wavelength, and three digit day references are references to the sequential day of the year (February 1 being the 32nd day of the year). The method of Evans was used for total radiance correction which is unpublished but briefly discussed in McClain et al. (1992).

Table 2. Level-2 processing parameters.

Parameter	Value
Level-1 Image Name:	SNG:5106Bx.IMG
Level-2 Image Name:	Y4NG:5106B-0-L2x.IMG
Processing Day/Time:	15-Oct-1991/14:21:33
Orbit Number:	5106
Tilt Angle:	10.000
Sensor Gain:	1
Wavelengths:	443, 520, 550, 550, 670 nm
Scene Year/Day/Time:	1979/301/16.766
Thresholds	
Land/Cloud (750 nm):	21 counts
Haze (670 nm):	255 counts
Pigment Algorithm:	Two Channel[1]
Water Radiances:	Normalized
Water Rad. Range:	0.0, 3.0
Rayleigh Calculations:	Exact[2]
Mean Solar Flux:	186.96, 187.02, 186.81, 153.09
Optical Thicknesses	
Ozone:	0.0011, 0.0144, 0.0279, 0.0125
Rayleigh:	0.237, 0.123, 0.098, 0.044
Ångström Coefficients:	0.0, 0.0, 0.0
Epsilon Coefficients:	1.0, 1.0, 1.0
ILT Record Option:	Yes
Solar Zenith Angle:	44.491° (at center)
Satellite Zenith Angle:	11.370° (at center)
Solar Azimuth Angle:	95.673° (at center)
Satellite Azim. Angle:	290.502° (at center)
Total Rad. Correction:	Method of R. Evans[3]
Water Rad. Iteration:	None[4]

1. Gordon et al. 1983.
2. Gordon et al. 1988.
3. Unpublished.
4. Smith and Wilson 1981.

3. RESULTS

COLOR PLATES 1–8 (see envelope on back of cover for all PLATES) show the pigment images for the full-resolution processing, Methods 1–4, and Methods 6–8, respectively. Of these images, the most striking is PLATE 2 for Method 1 which shows GAC blocks with high pigment values in the Gulf Steam and Sargasso Sea regions. Apparently, these high values are artifacts of the imperfect cloud detection threshold. In all cases, the high values are isolated, occur in the vicinity of a cloud, and always produce pigment values of 39 mg m^{-3} (a grey level of 254 based on SEAPAK's scaling convention). Most cases are associated with the small scattered clouds over the Gulf Stream and not the larger cloud bank along the eastern portion of the image. Therefore, the problem does not appear to be related to sensor ringing, but is possibly related to subpixel size clouds. Generally, the effect results in low normalized water-leaving radiances in the 443, 520, and 550 nm

Table 3. Statistical summary of various methods. Analyses of the full resolution are labeled "Full". Because the GAC methods fill the entire 16 pixel block with constant values, the "Valid Count" is not the true number of independent pixel pairs.

Parameter	Cross-correlation Between Methods	Cross-correlation Coefficient	Mean Value	Standard Deviation	Valid Count
$L_{WN}(443)$	Full		1.527	0.759	131,413
	2		1.518	0.757	131,344
	2 and 1	0.777	1.584	0.780	164,160
	2 and 3	0.772	1.566	0.798	164,160
	2 and 4	0.755	1.752	0.848	164,160
	2 and 6	0.760	1.686	0.831	164,160
$L_{WN}(520)$	Full		0.807	0.386	131,413
	2		0.801	0.378	131,344
	2 and 1	0.568	0.874	0.447	164,160
	2 and 3	0.567	0.867	0.453	164,160
	2 and 4	0.581	1.033	0.555	164,160
	2 and 6	0.531	0.936	0.478	164,160
$L_{WN}(550)$	Full		0.505	0.235	131,413
	2		0.503	0.231	131,344
	2 and 1	0.757	0.511	0.223	164,160
	2 and 3	0.755	0.507	0.225	164,160
	2 and 4	0.677	0.558	0.217	164,160
	2 and 6	0.687	0.547	0.234	164,160
$L_a(670)$	Full		0.467	0.367	131,413
	2		0.468	0.363	131,344
	2 and 1	0.512	0.527	0.290	164,160
	2 and 3	0.511	0.525	0.291	164,160
	2 and 4	0.261	0.310	0.226	164,160
	2 and 6	0.283	0.351	0.223	164,160
Pigment Concentration	Full		1.320	5.343	131,413
	2		1.364	5.471	131,344
	2 and 1	0.411	2.046	6.149	164,160
	2 and 3	0.358	1.405	5.537	164,160
	2 and 4	0.268	1.108	4.664	164,160
	2 and 6	0.300	1.176	4.790	164,160
	2 and 7	0.356	1.370	5.462	164,160
	2 and 8	0.341	1.294	5.026	164,160

derived products. Because of the lower number of valid values in a GAC block containing clouds, the weight of the high value is amplified which biases the average pigment value of the scene to higher values and dramatically modifies the frequency distribution as discussed below.

Histograms of the level-2 images were generated using the SEAPAK program HIST. Pixels flagged as being land, clouds or saturated in the 670 nm band were excluded from the analyses. The histograms in Figs. 1–4 compare the frequency distributions of the normalized water-leaving radiances [$L_{WN}(443)$, $L_{WN}(520)$, $L_{WN}(550)$] and aerosol radiance [$L_a(670)$] for the full-resolution and Method 2 products. The histograms of Figs. 5–11 compare the frequency distributions of pigment concentration for the full-resolution data and the seven GAC methods. The comparison of the full-resolution and Method 2 histograms show high fidelity as would be expected, but with some scatter due to the fact that Method 2 has a greatly reduced number of valid samples. Methods 1, 3, 4, 6, 7, and 8 all show elevated peaks at low pigment concentrations. Also, note the histogram minimum at 1.5 mg m^{-3} in all pigment histograms except Methods 1 and 8. This is due to the algorithm switching mechanism in the two-channel bio-optical algorithm (Denman and Abbott 1988; Muller-Karger et al. 1990). Methods 3, 4, 6, and 7 clearly tend to over estimate pigment concentrations for the range above 1.5 mg m^{-3}. Method 1 produces greatly exaggerated values at high concentrations while Method 8 results in reasonably good estimates in this concentration range. Scatterplots of the data products from Methods 1, 3, 4,

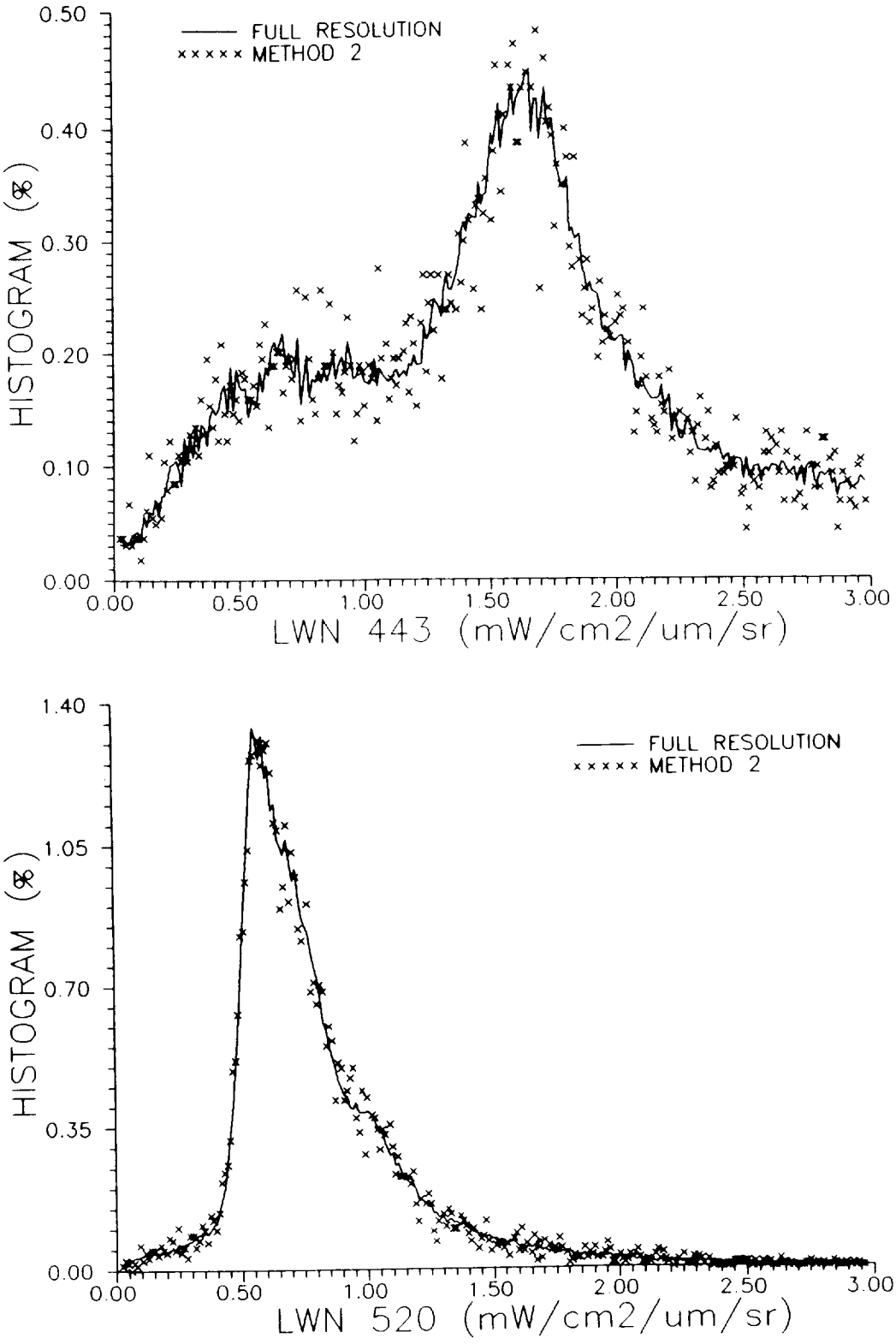

Figs. 1 and 2. Histograms comparing the distributions of $L_{WN}(443)$ [top] and $L_{WN}(520)$ [bottom], respectively, as derived from the full resolution and Method 2 analyses.

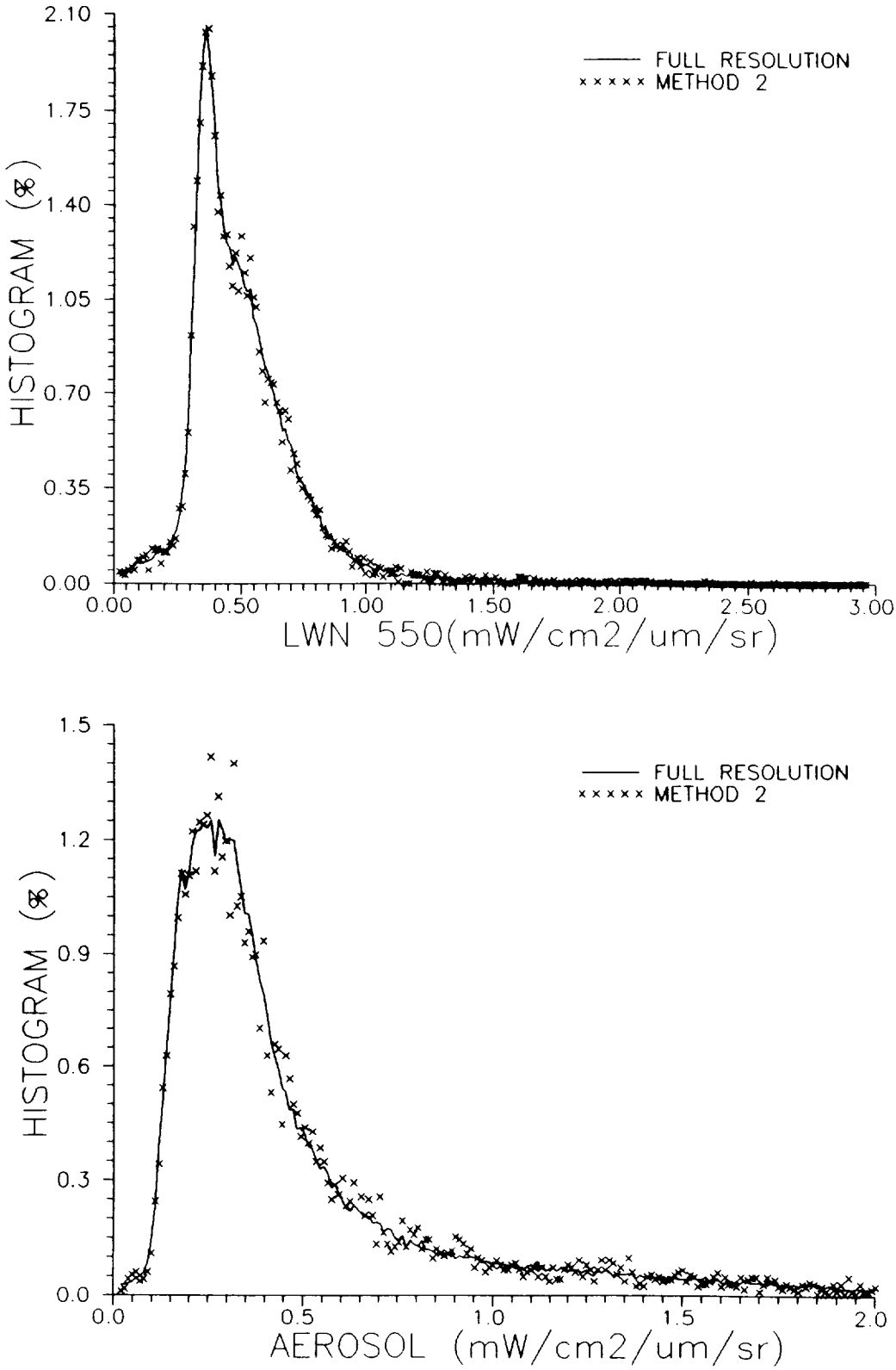

Figs. 3 and 4. Histograms comparing the distributions of $L_{WN}(550)$ [top] and L_a [bottom], respectively, as derived from the full resolution and Method 2 analyses.

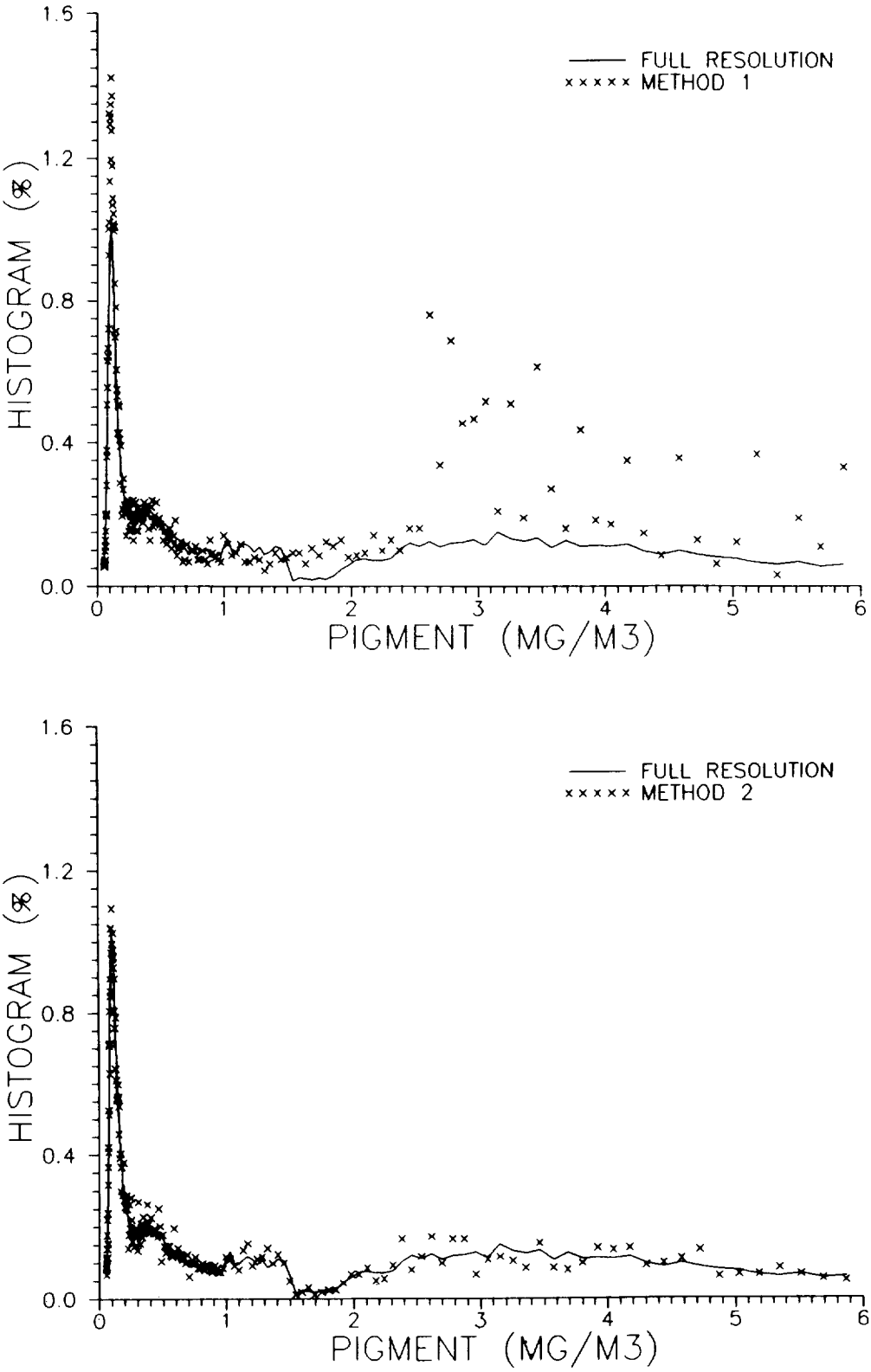

Figs. 5 and 6. Histograms comparing the pigment concentrations of the full resolution analysis with those obtained from Methods 1 [top] and 2 [bottom], respectively.

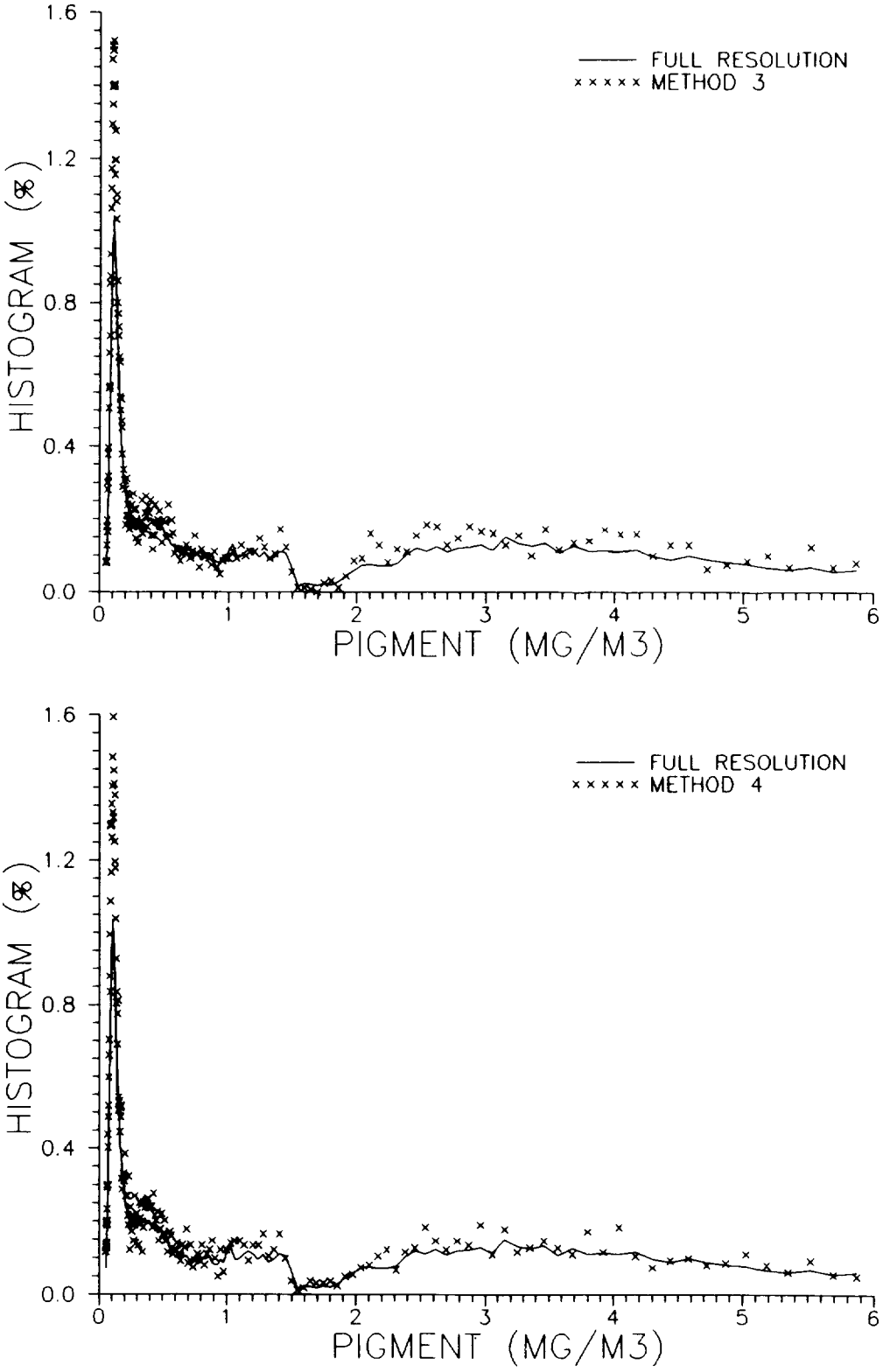

Figs. 7 and 8. Histograms comparing the pigment concentrations of the full resolution analysis with those obtained from Methods 3 [top] and 4 [bottom], respectively.

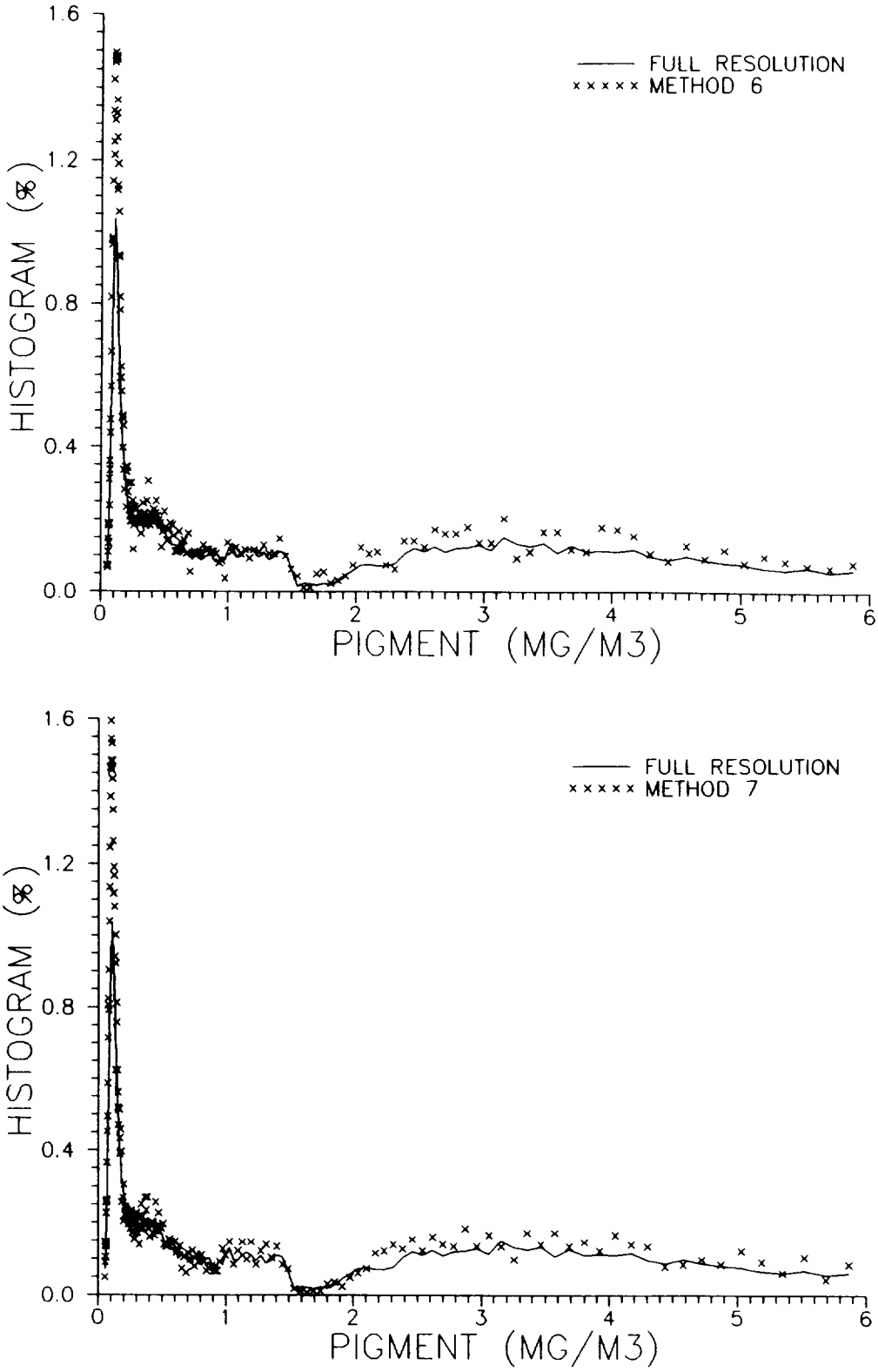

Figs. 9 and 10. Histograms comparing the pigment concentrations of the full resolution analysis with those obtained from Methods 6 [top] and 7 [bottom], respectively.

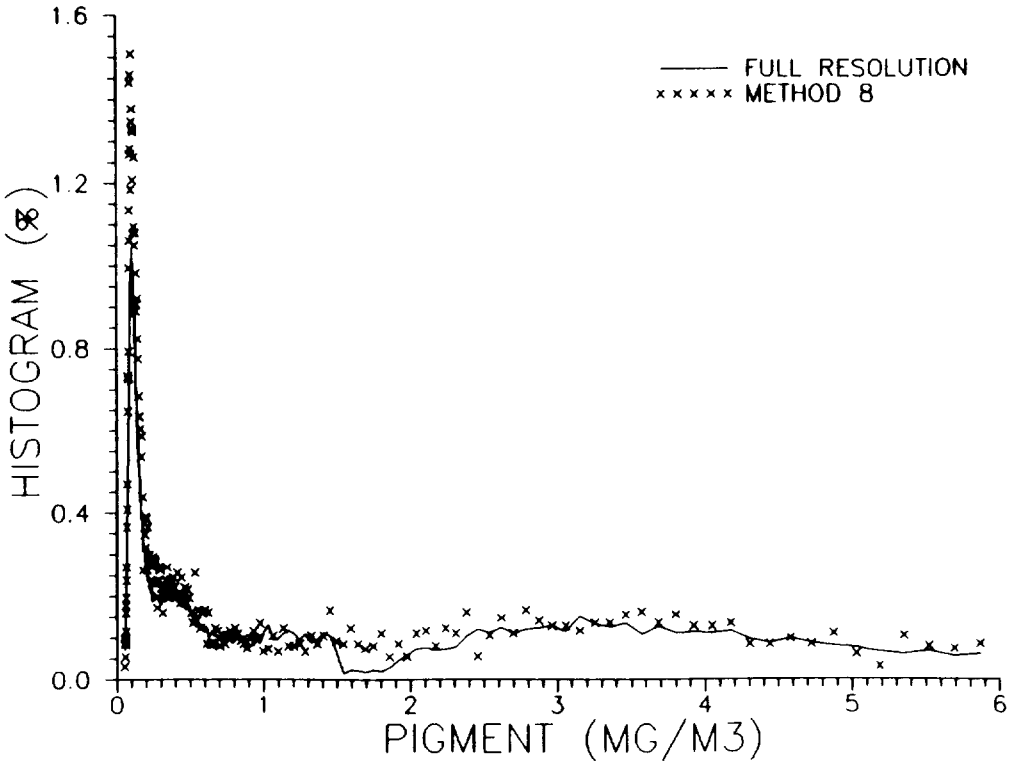

Fig. 11. Histogram comparing the pigment concentrations of the full resolution analysis with those obtained from Method 8.

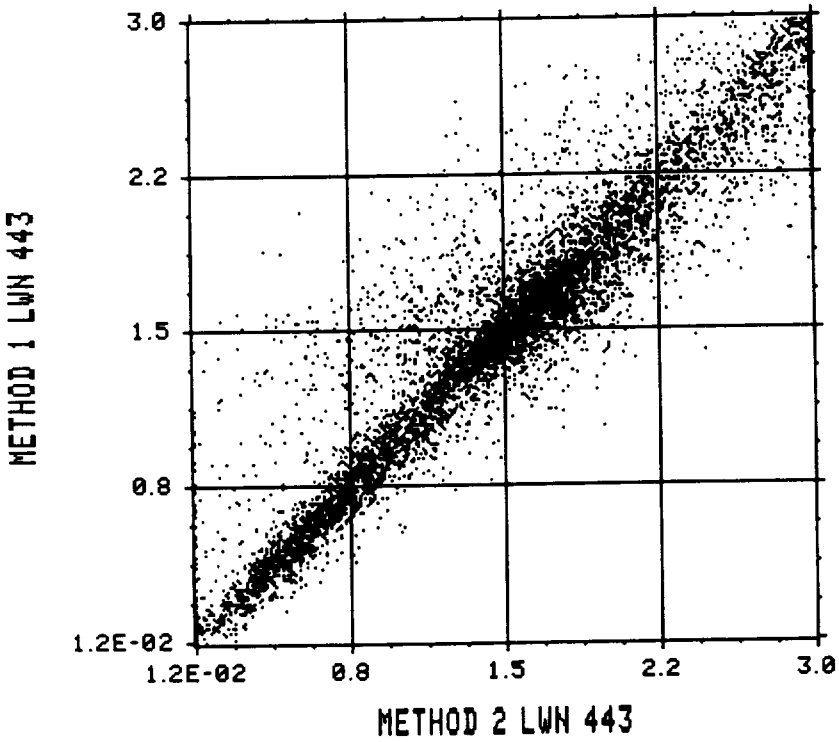

Fig. 12. Scatterplot comparing the $L_{WN}(443)$ obtained from Methods 1 and 2.

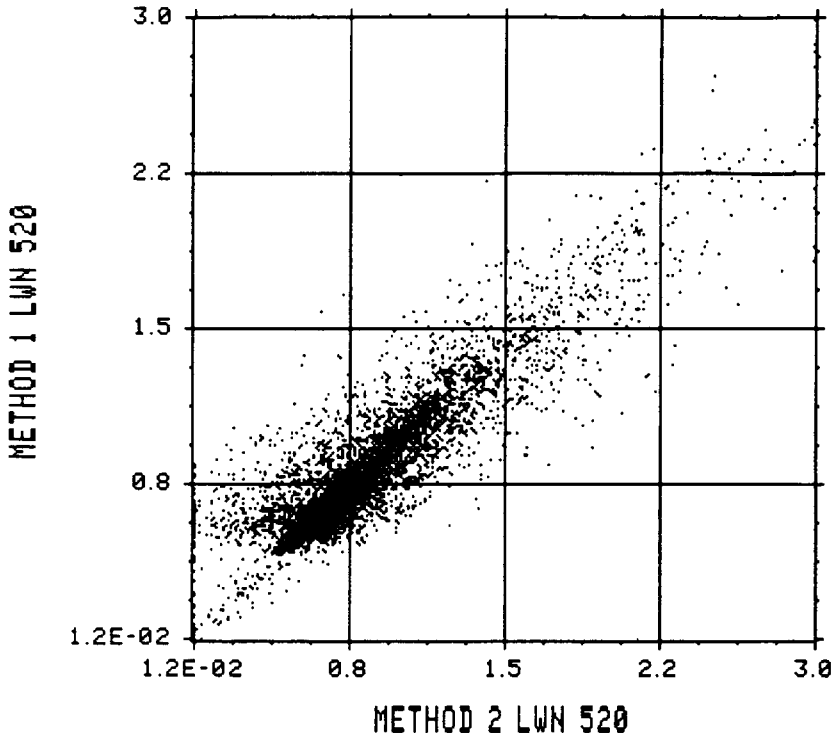

Fig. 13. Scatterplot comparing the $L_{WN}(520)$ obtained from Methods 1 and 2.

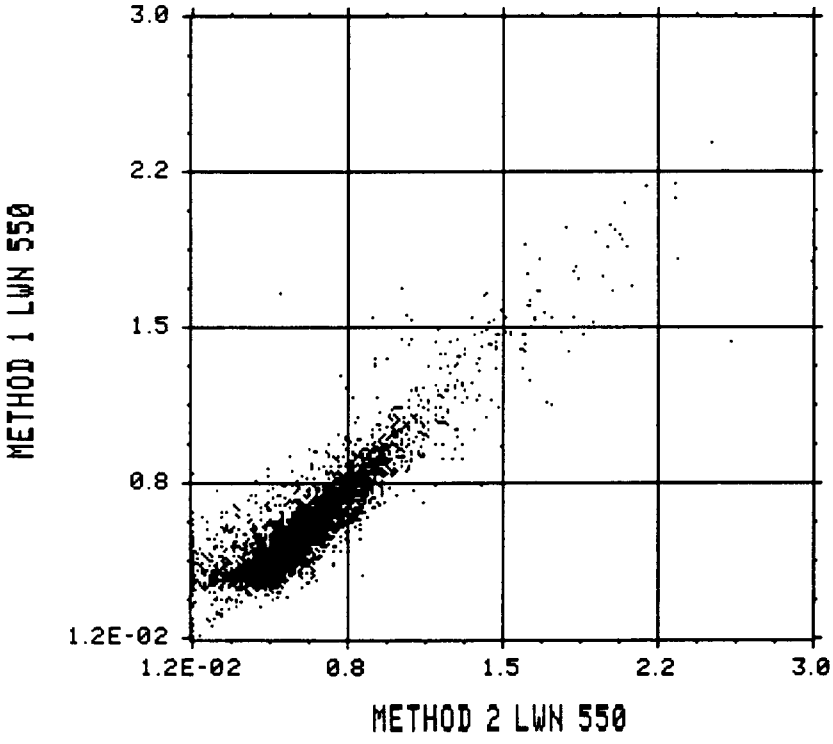

Fig. 14. Scatterplot comparing the $L_{WN}(550)$ obtained from Methods 1 and 2.

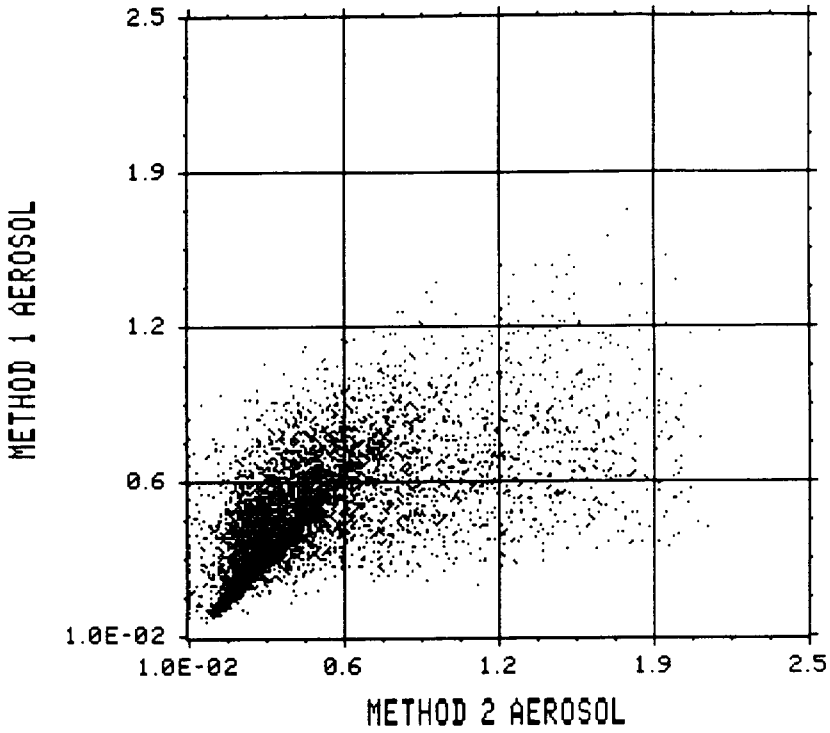

Fig. 15. Scatterplot comparing the L_a obtained from Methods 1 and 2.

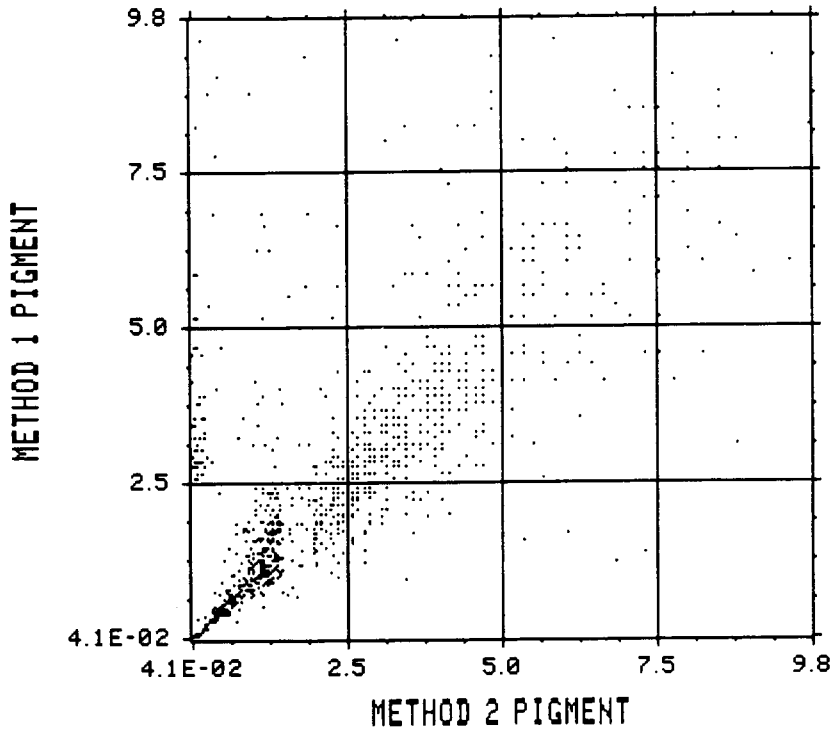

Fig. 16. Scatterplot comparing the pigment values obtained from Methods 1 and 2.

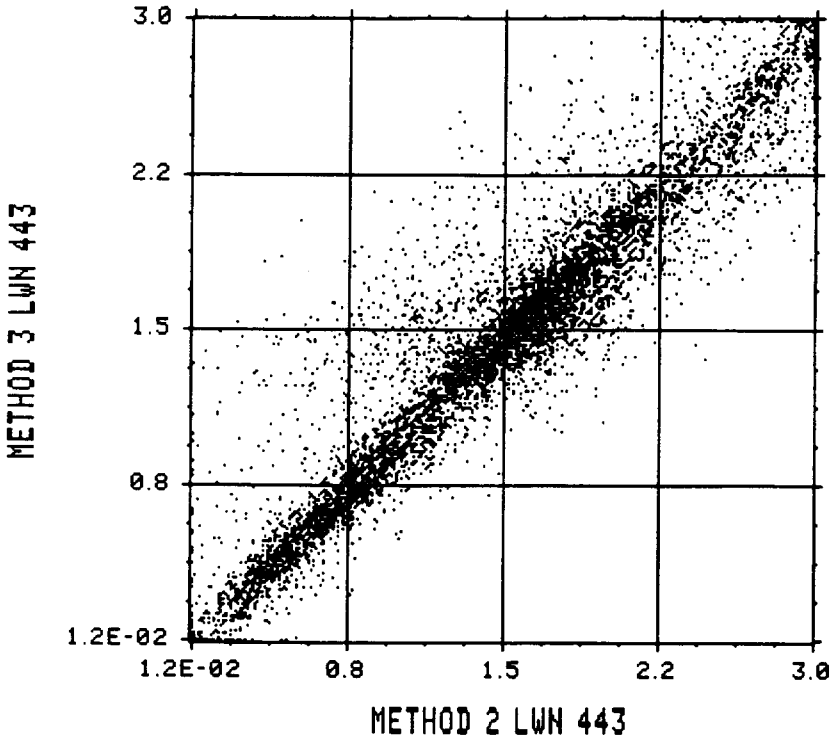

Fig. 17. Scatterplot comparing the $L_{WN}(443)$ obtained from Methods 3 and 2.

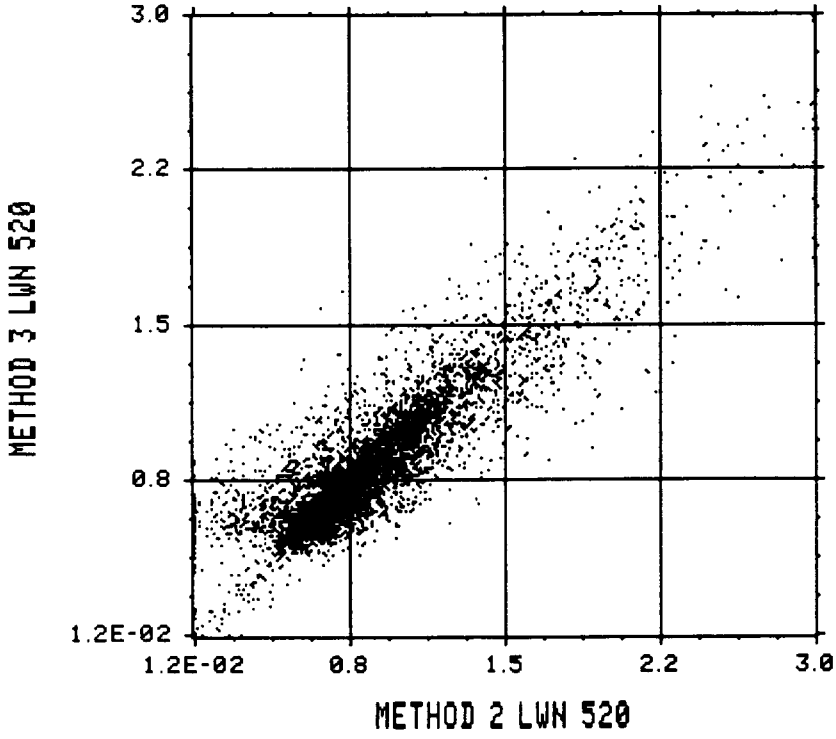

Fig. 18. Scatterplot comparing the $L_{WN}(520)$ obtained from Methods 3 and 2.

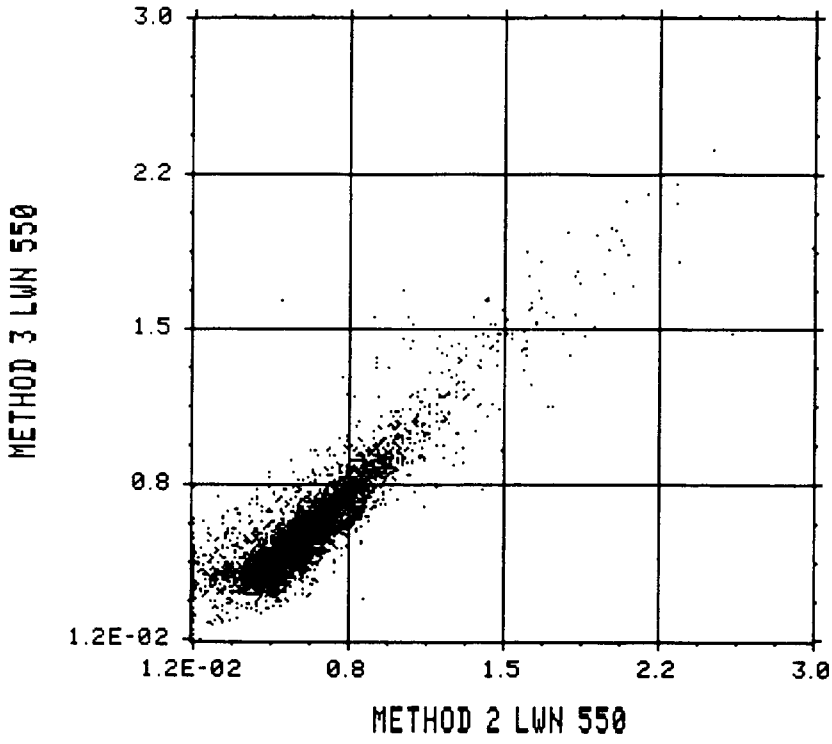

Fig. 19. Scatterplot comparing the $L_{WN}(550)$ obtained from Methods 3 and 2.

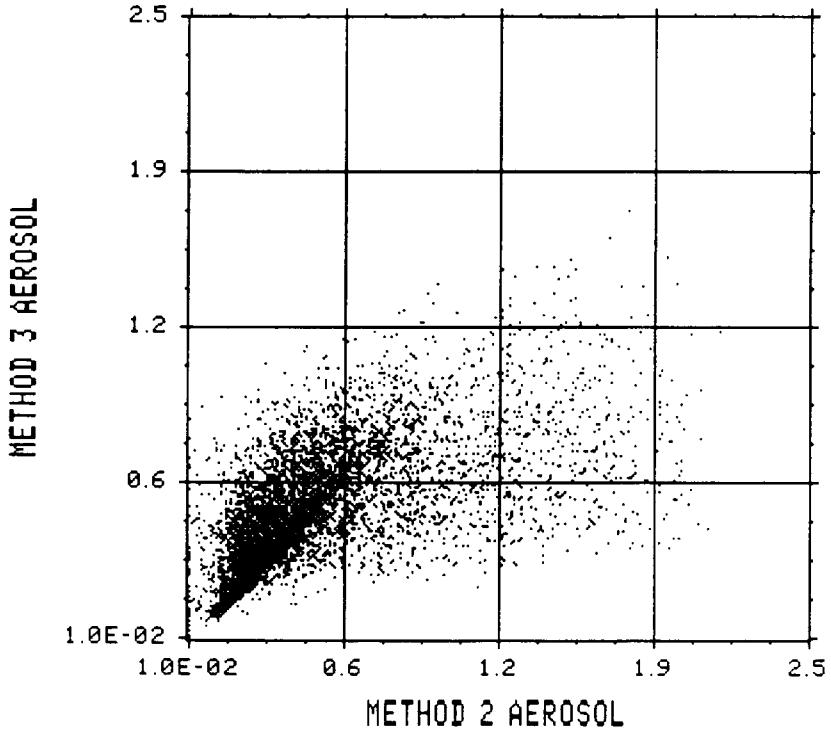

Figs. 20. Scatterplot comparing the L_a obtained from Methods 3 and 2.

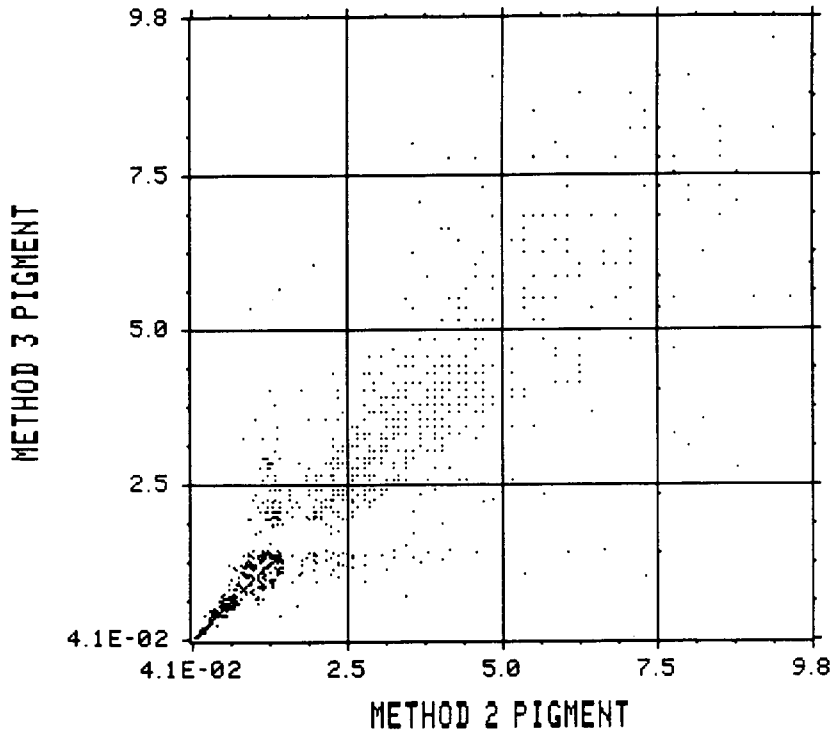

Fig. 21. Scatterplot comparing the pigment values obtained from Methods 3 and 2.

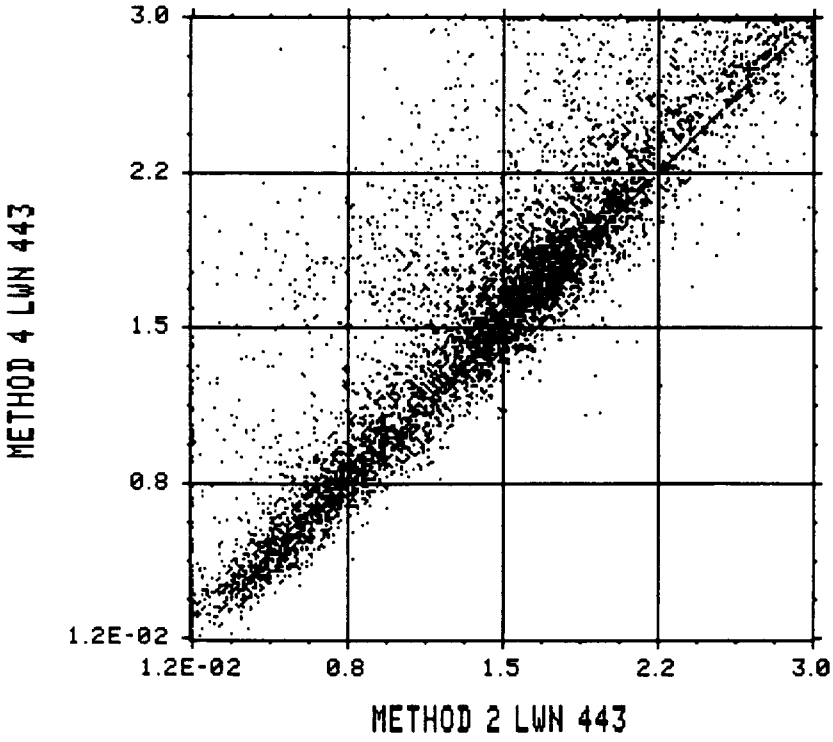

Fig. 22. Scatterplot comparing the $L_{WN}(443)$ obtained from Methods 4 and 2.

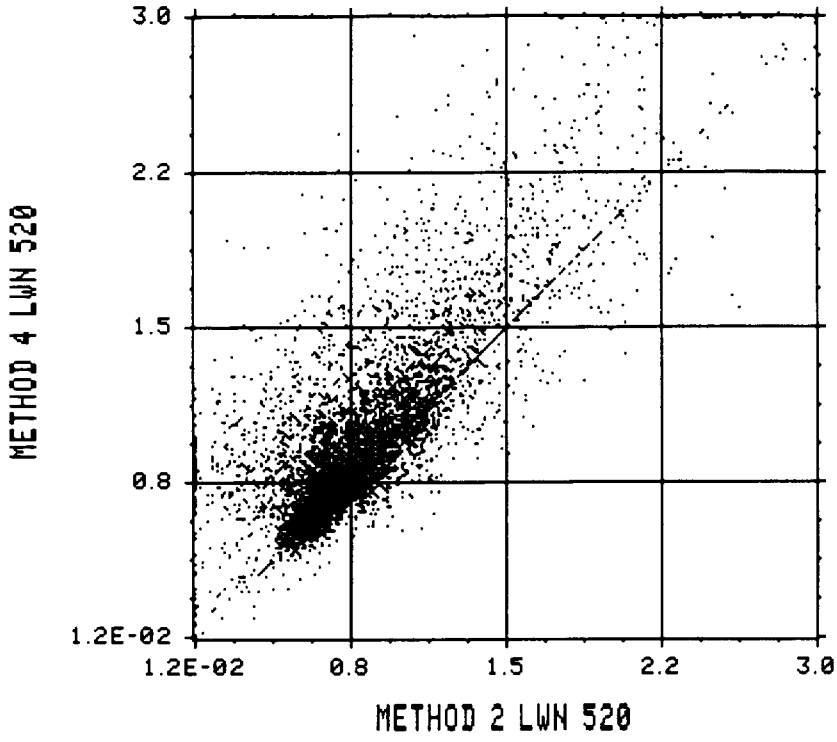

Fig. 23. Scatterplot comparing the $L_{WN}(520)$ obtained from Methods 4 and 2.

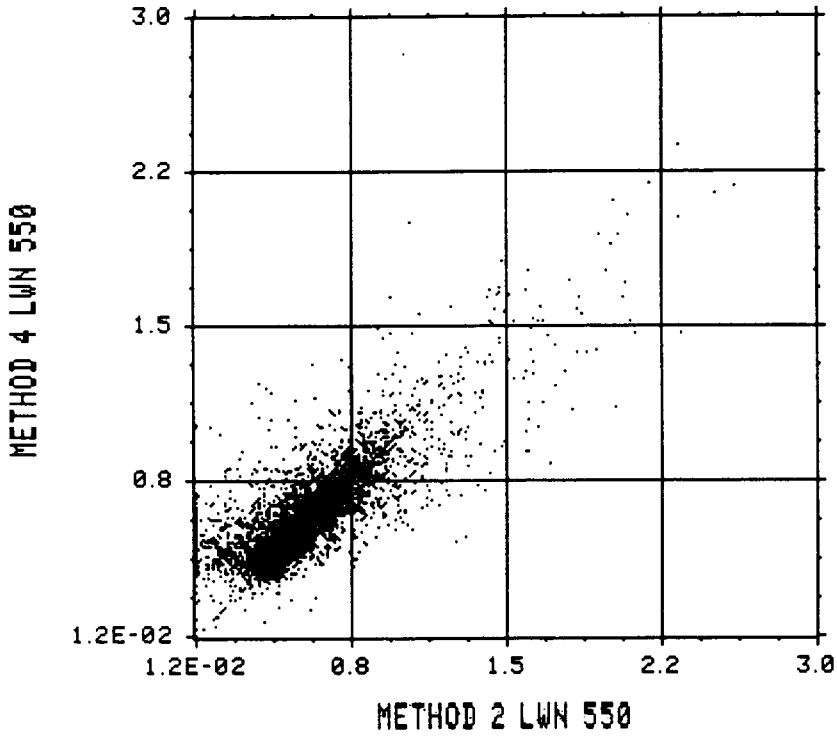

Fig. 24. Scatterplot comparing the $L_{WN}(550)$ obtained from Methods 4 and 2.

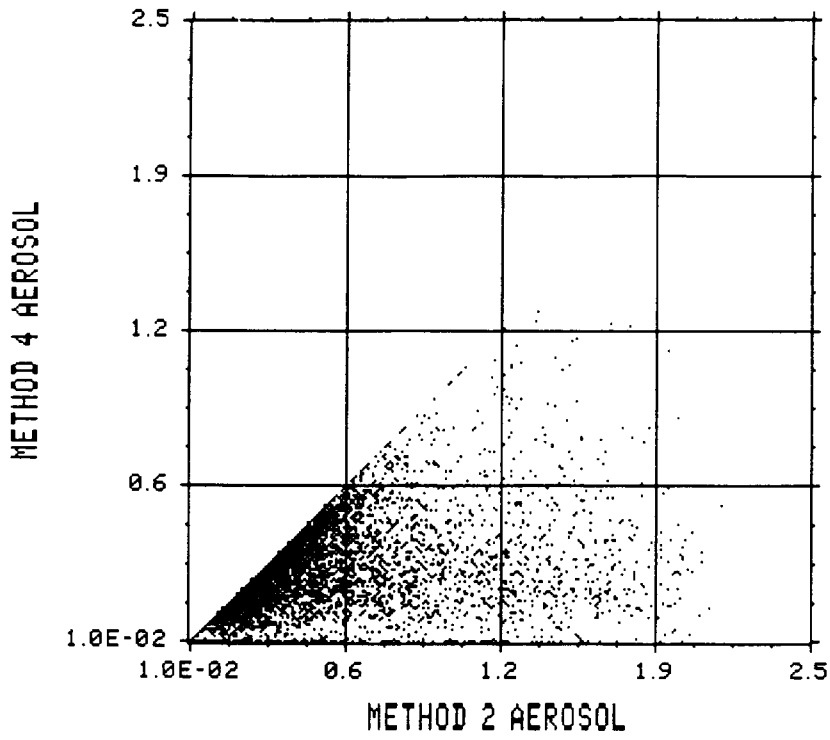

Fig. 25. Scatterplot comparing the L_a obtained from Methods 4 and 2.

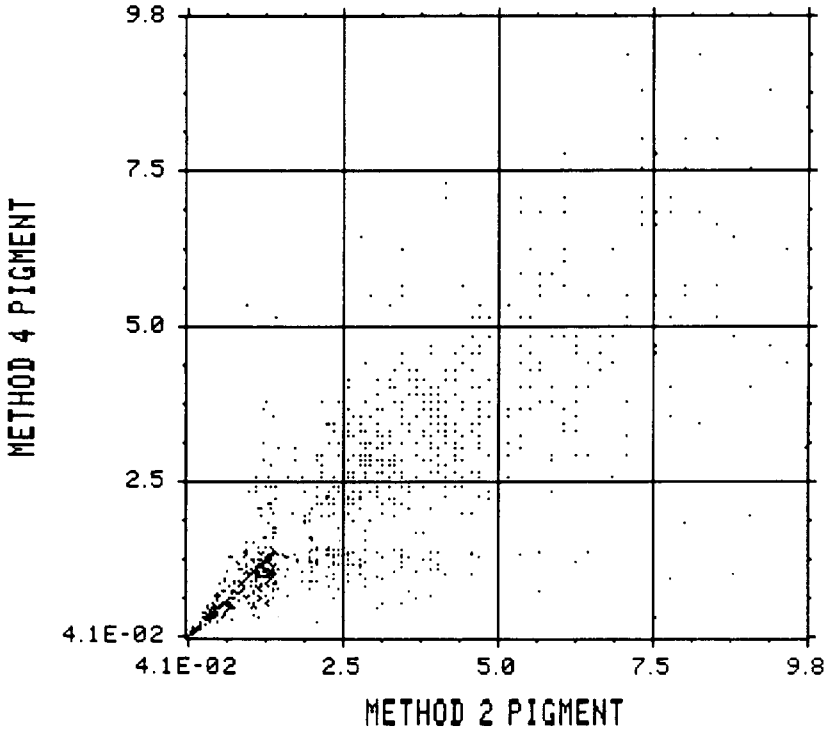

Fig. 26. Scatterplot comparing the pigment values obtained from Methods 4 and 2.

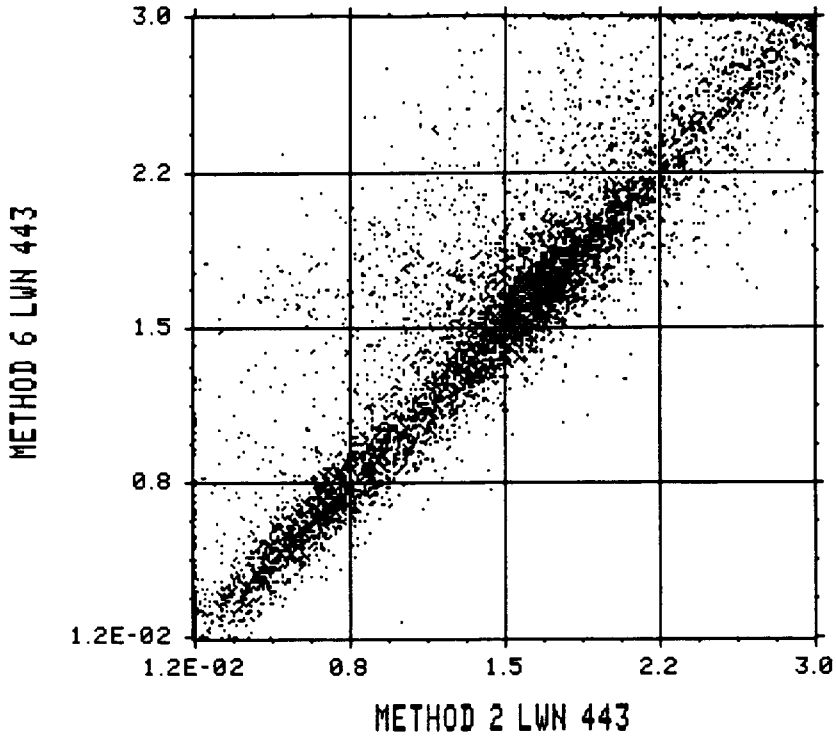

Fig. 27. Scatterplot comparing the $L_{WN}(443)$ obtained from Methods 6 and 2.

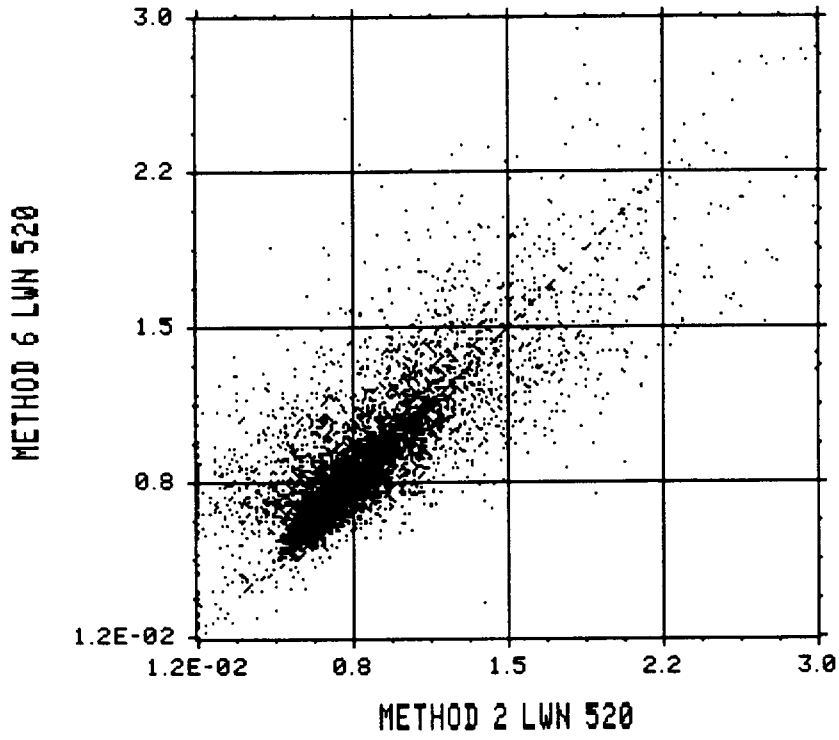

Fig. 28. Scatterplot comparing the $L_{WN}(520)$ obtained from Methods 6 and 2.

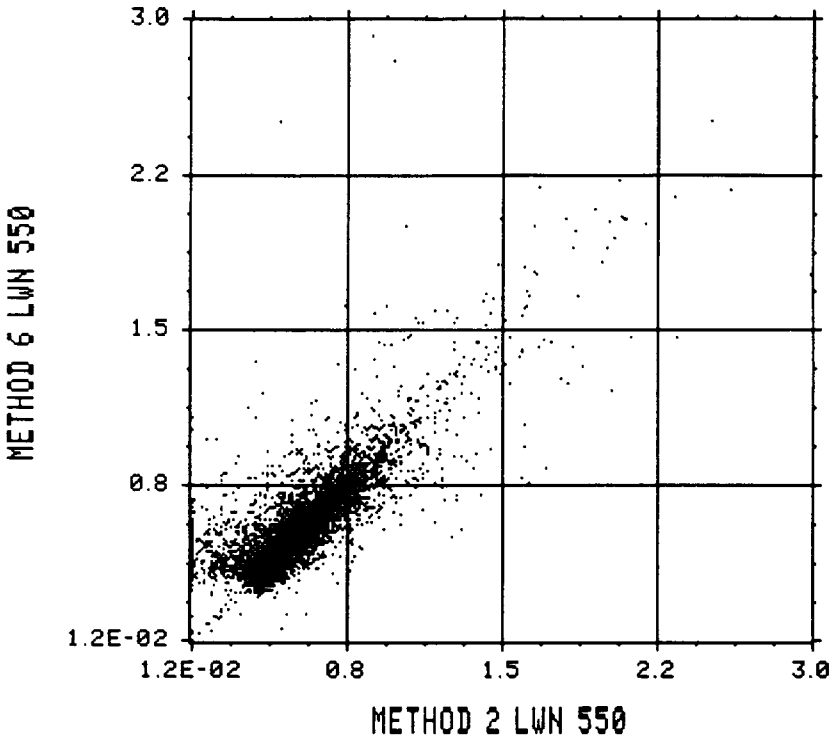

Fig. 29. Scatterplot comparing the $L_{WN}(550)$ obtained from Methods 6 and 2.

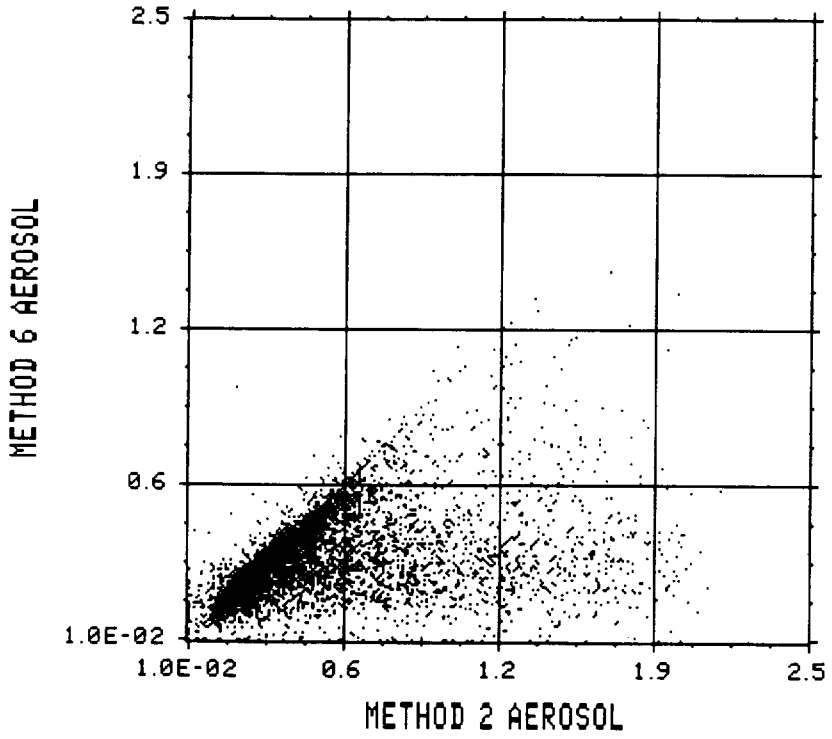

Fig. 30. Scatterplot comparing the L_a obtained from Methods 6 and 2.

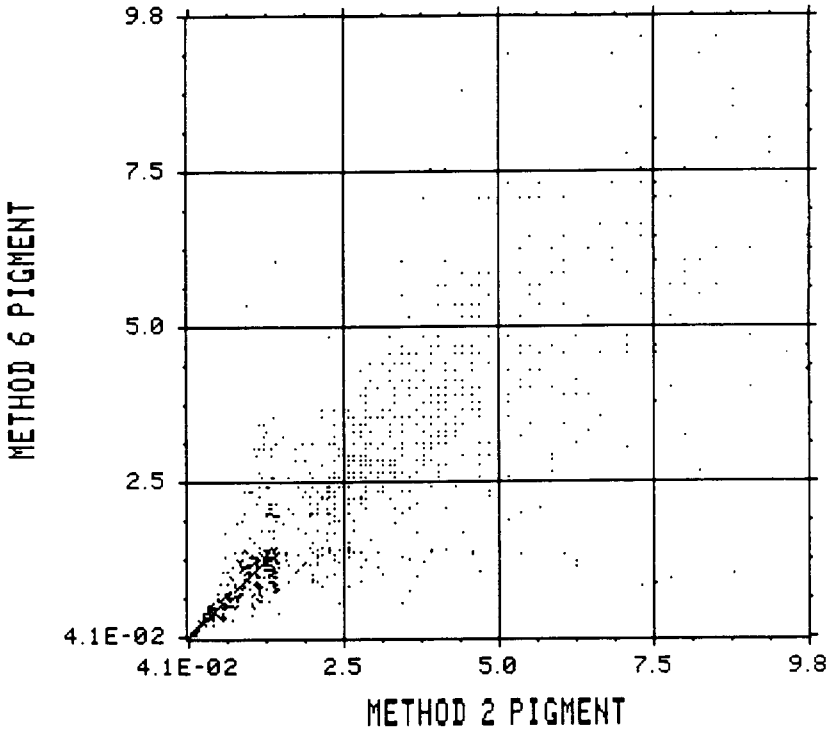

Fig. 31. Scatterplot comparing the pigment values obtained from Methods 6 and 2.

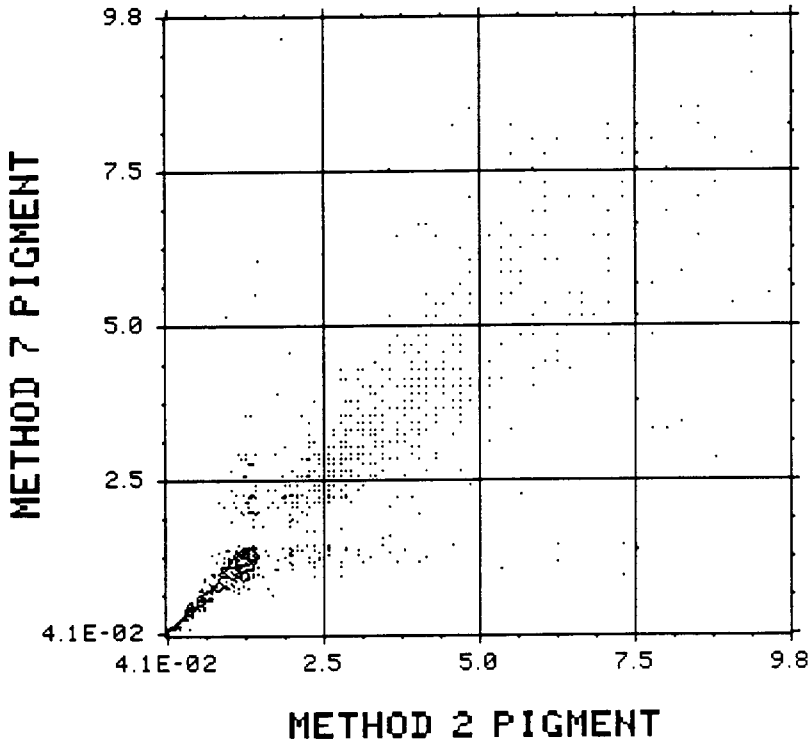

Fig. 32. Scatterplot of pigment values from Methods 7 and 2.

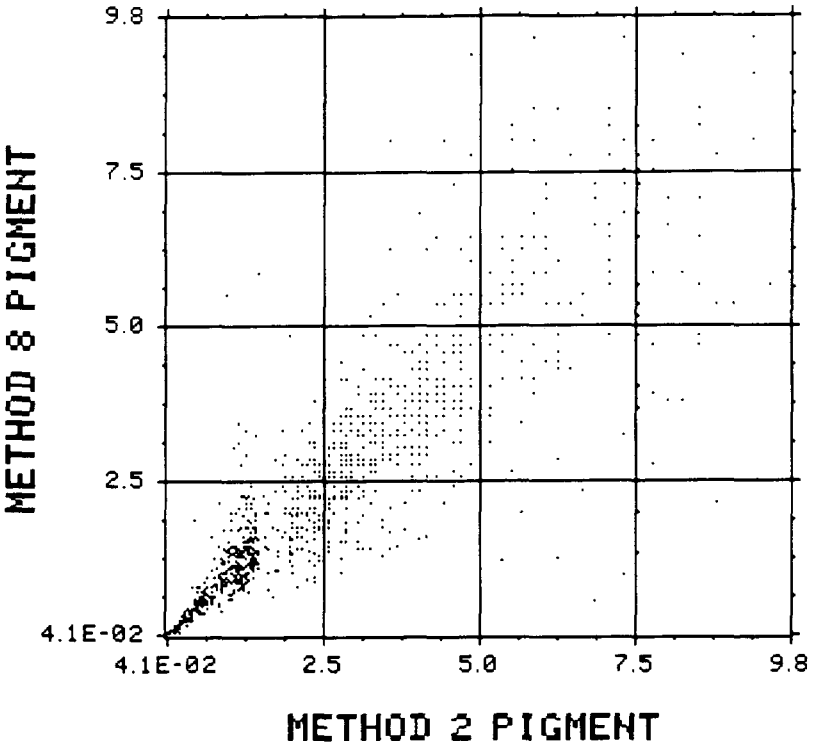

Fig. 33. Scatterplot of pigment values from Methods 8 and 2.

Scatterplots of the data products from Methods 1, 3, 4, 6, 7, and 8 versus Method 2 are shown in Figs. 12–16, 17–21, 22–26, 27–31, 32, and 33, respectively. Only pigment comparisons are shown for Methods 7 and 8 because both are derived from Method 1 products. Method 2 was used as the baseline for evaluation because it most closely represents the the full resolution image as shown in the histograms. The SEAPAK program SCATT was used to generate the scatterplots. SCATT excludes any pixel pair that includes a value outside the range of valid values. All methods tend to yield high values of $L_{WN}(443)$, especially Methods 4 and 6, the least-value methods. For $L_{WN}(520)$, the bias towards high values is especially pronounced with Method 4. As expected, Methods 4 and 6 strongly bias $L_a(670)$ towards low values. Finally, the pigment scatterplots do not indicate any pronounced biases, which are better illustrated in the frequency distribution plots and quantified in Table 3.

The last analysis performed used the SEAPAK program CORCO to determine the image's first and second statistical moments and the correlation statistics between Methods 1, 3, 4, and 6 versus Method 2. The statistics are presented in Table 3. The statistics for full resolution products (no subsampling; labeled "Full" in Table 3) and Method 2 products were computed using the same image for the two image inputs required by CORCO, so cross-correlation coefficients for these cases are meaningless.

4. DISCUSSION

As indicated in the histograms, Table 3, and the scatterplots, the average-value and least-value techniques tend to overestimate the normalized radiances with the least-value value methods performing the worst. Additionally, the relative increases in normalized water radiances are highest at 520 nm and lowest at 550 nm. However, as indicated in the pigment histograms, this does not necessarily hold for all water masses in the scene. The tendency in the pigment range above 1.5 mg m^{-3} is to overestimate the concentrations and requires the relative increase in $L_W(550)$ be greater than in $L_W(520)$. As expected, the least-value methods bias the aerosol radiances towards lower values. On the other hand, the average-value methods bias the aerosol radiances toward high values. Also, the least-value methods underestimate the mean pigment concentrations.

In summary, the fixed pixel subsampling gives the best representation of the full resolution data for GAC product generation. The explanation for why the water-radiances are biased in one direction, or the other, depending on water mass, is more involved and is beyond the scope of this analysis.

Glossary

AVHRR	Advanced Very High Resolution Radiometer
CZCS	Coastal Zone Color Scanner
GAC	Global Area Coverage
LAC	Local Area Coverage
NOAA	National Oceanic and Atmospheric Administration
SEAPAK	Software package developed at NASA/Goddard Space Flight Center which ingests, displays, and processes data from the CZCS
SeaWiFS	Sea-viewing Wide Field-of-view Sensor
TOMS	Total Ozone Mapping Spectrometer

References

Denman, K.L. and M.R. Abbott, 1988: Time evolution of surface chlorophyll patterns from cross spectrum analysis of satellite color images, *J. Geophys. Res.,* **93,** 6,789–6,798.

Gordon, H.R., D.K. Clark, J.W. Brown, O.B. Brown, R.H. Evans, and W.W. Broenkow, 1983: Phytoplankton pigment concentrations in the Middle Atlantic Bight: Comparison of ship determinations and CZCS estimates, *Appl. Opt.,* **22,** 20–36.

——, J.W. Brown, and R.H. Evans, 1988: Exact Rayleigh scattering calculations for use with the Nimbus-7 Coastal Zone Color Scanner, *Appl. Opt.,* **27,** 862–871.

Justice, J.O., B.L. Markham, J.R.G. Townshend, and R.L. Kennard, 1989: Spatial degradation of satellite data, *Int. J. Remote Sensing,* **10,** 1,539–1,561.

McClain, C.R., M. Darzi, J. Firestone, E. Yeh, G. Fu, and D. Endres, 1991a: SEAPAK Users Guide, Version 2.0, Vol. I—System Description, NASA/Goddard Space Flight Center, *NASA Tech. Memo. 100728,* 158 pp.

——, M. Darzi, J. Firestone, E. Yeh, G. Fu, and D. Endres, 1991b: SEAPAK Users Guide, Version 2.0, Vol. II—Descriptions of Programs NASA/Goddard Space Flight Center, *NASA Tech. Memo. 100728,* 586 pp.

——, W.E. Esaias, W. Barnes, B. Guenther, D. Endres, S.B. Hooker, G. Mitchell, and R. Barnes, 1992: Calibration and Validation Plan for SeaWiFS, *NASA Tech. Memo. 104566, Vol. 3,* S.B. Hooker and E.R. Firestone, Eds., 41 pp.

Morel, A., and L. Prieur, 1977: Analysis of variations in ocean color, *Limnol. Oceanogr.,* **22,** 709–722.

Mueller, J.L., 1988: Nimbus–7 CZCS: Electronic overshoot due to cloud reflectance, *Appl. Opt.,* **27,** 438–440.

Muller-Karger, F.E., C.R. McClain, R.N. Sambrotto, and G.C. Ray, 1990: A comparison of ship and CZCS-mapped distributions of phytoplankton in the Southeastern Bering Sea, *J. Geophys. Res.,* **95,** 483–499.

Smith, R.C., and W.H. Wilson, 1981: Ship and satellite bio-optical research in the California Bight, *Oceanography from Space,* J.F.R. Gower, Ed., Plenum Press, 281-294.

REPORT DOCUMENTATION PAGE

Form Approved
OMB No. 0704-0188

1. AGENCY USE ONLY *(Leave blank)*	2. REPORT DATE	3. REPORT TYPE AND DATES COVERED
	November 1992	Technical Memorandum

4. TITLE AND SUBTITLE
SeaWiFS Technical Report Series
Volume 4, An Analysis of GAC Sampling Algorithms:
A Case Study

5. FUNDING NUMBERS
970.2

6. AUTHOR(S)
Charles R. McClain, Eueng-nan Yeh, and Gary Fu

Series Editors: Stanford B. Hooker and Elaine R. Firestone

7. PERFORMING ORGANIZATION NAME(S) AND ADDRESS(ES)
Laboratory for Hydrospheric Processes
Goddard Space Flight Center
Greenbelt, Maryland 20771

8. PERFORMING ORGANIZATION REPORT NUMBER
93B00016

9. SPONSORING/MONITORING AGENCY NAME(S) AND ADDRESS(ES)
National Aeronautics and Space Administration
Washington, D.C. 20546-0001

10. SPONSORING/MONITORING AGENCY REPORT NUMBER
TM-104566, Vol. 4

11. SUPPLEMENTARY NOTES
E. Yeh, G. Fu, and E. Firestone: General Sciences Corporation, Laurel, Maryland.

12a. DISTRIBUTION/AVAILABILITY STATEMENT
Unclassified - Unlimited
Subject Category 48

12b. DISTRIBUTION CODE

13. ABSTRACT *(Maximum 200 words)*
The Sea-viewing Wide Field-of-View Sensor (SeaWiFS) instrument will sample at approximately a 1-km resolution at nadir, which will be broadcast for reception by realtime ground stations. However, the global data set will be comprised of coarser, 4-km data, which will be recorded and broadcast to the SeaWiFS Project for processing. Several algorithms for degrading the 1-km data to 4-km data are examined using imagery from the Coastal Zone Color Scanner (CZCS) in an effort to determine which algorithm would best preserve the statistical characteristics of the derived products generated from the 1-km data. Of the algorithms tested, subsampling based on a fixed pixel within a 4x4 pixel array is judged to yield the most consistent results when compared to the 1-km data products.

14. SUBJECT TERMS
Oceanography, SeaWiFS, Algorithms, GAC, SEAPAK, Pigment Concentration

15. NUMBER OF PAGES
20

16. PRICE CODE

17. SECURITY CLASSIFICATION OF REPORT	18. SECURITY CLASSIFICATION OF THIS PAGE	19. SECURITY CLASSIFICATION OF ABSTRACT	20. LIMITATION OF ABSTRACT
Unclassified	Unclassified	Unclassified	Unlimited

Color Plate Captions

Plate 1. Pigment concentration at full resolution using processing parameters provided in Table 2.

Plate 2. Pigment concentration at GAC resolution using Method 1 and processing parameters provided in Table 2.

Plate 3. Pigment concentration at GAC resoution using Method 2 and processing parameters provided in Table 2.

Plate 4. Pigment concentration at GAC resolution using Method 3 and processing parameters provided in Table 2.

Plate 5. Pigment concentration at GAC resolution using Method 4 and processing parameters provided in Table 2.

Plate 6. Pigment concentration at GAC resolution using Method 6 and processing parameters provided in Table 2.

Plate 7. Pigment concentration at GAC resolution using Method 7 and processing parameters provided in Table 2.

Plate 8. Pigment concentration at GAC resolution using Method 8 and processing parameters provided in Table 2.

PLATE 1

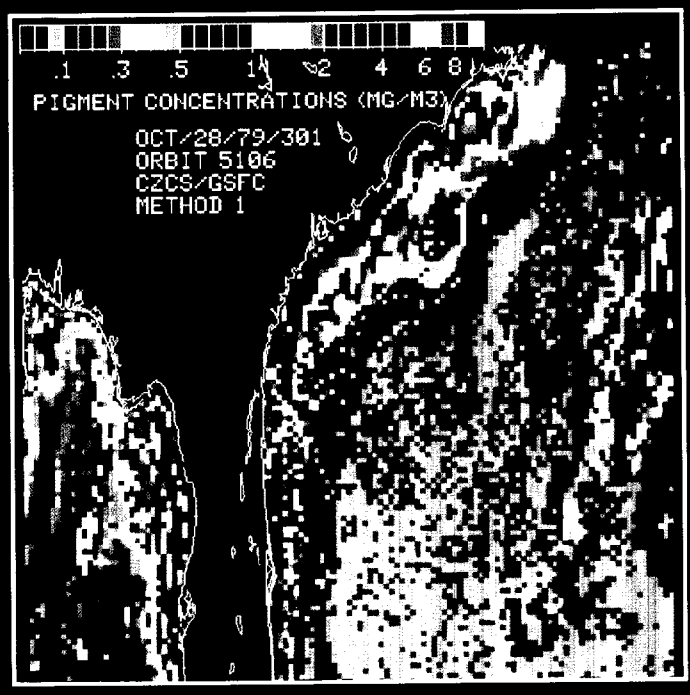

PLATE 2

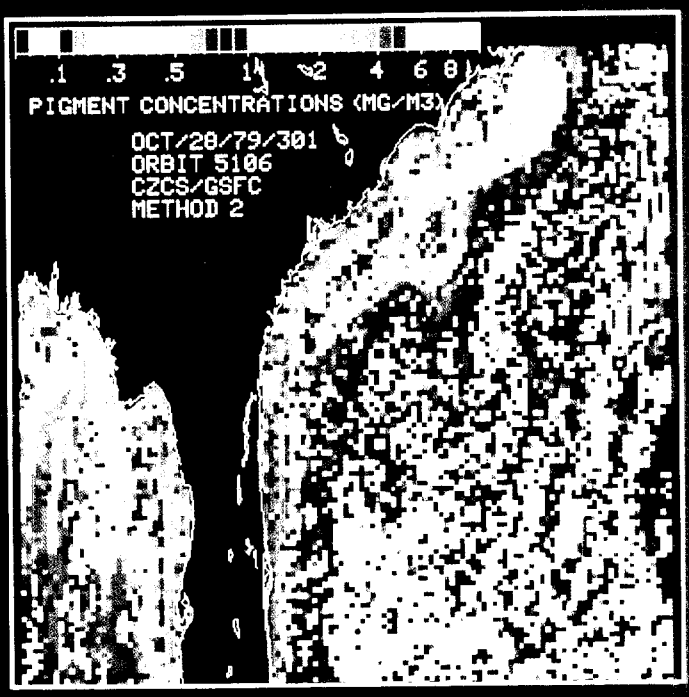

PLATE 3

PLATE 4

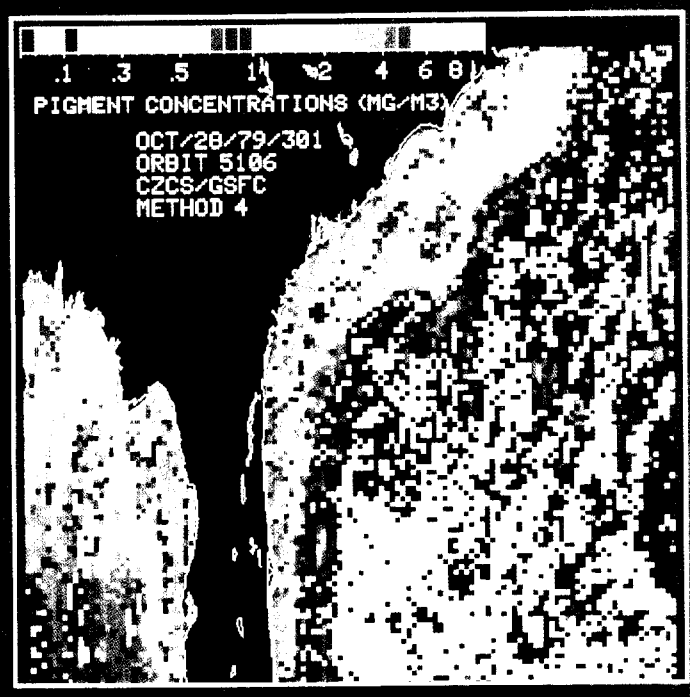

PLATE 5

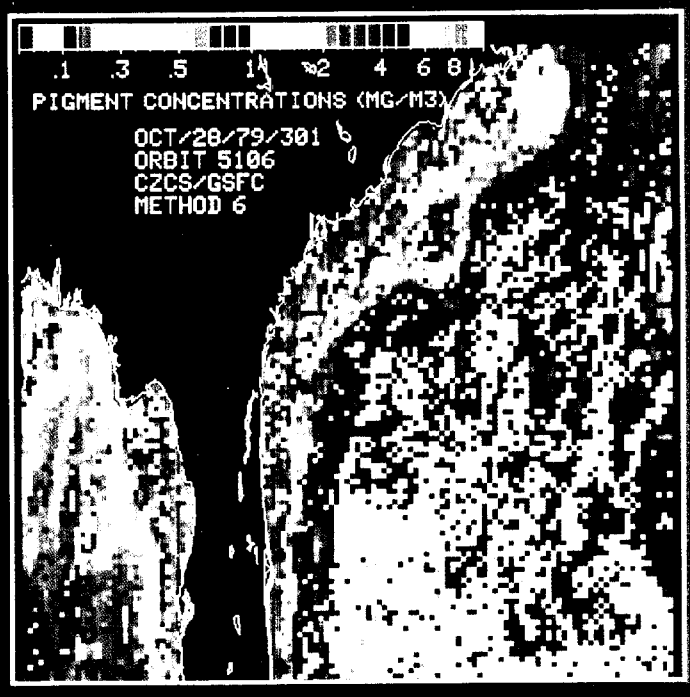

PLATE 6

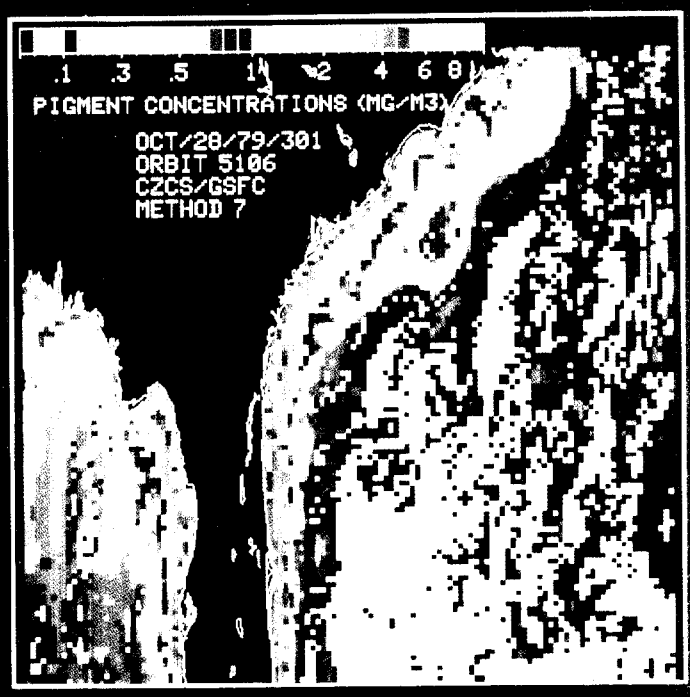

PLATE 7

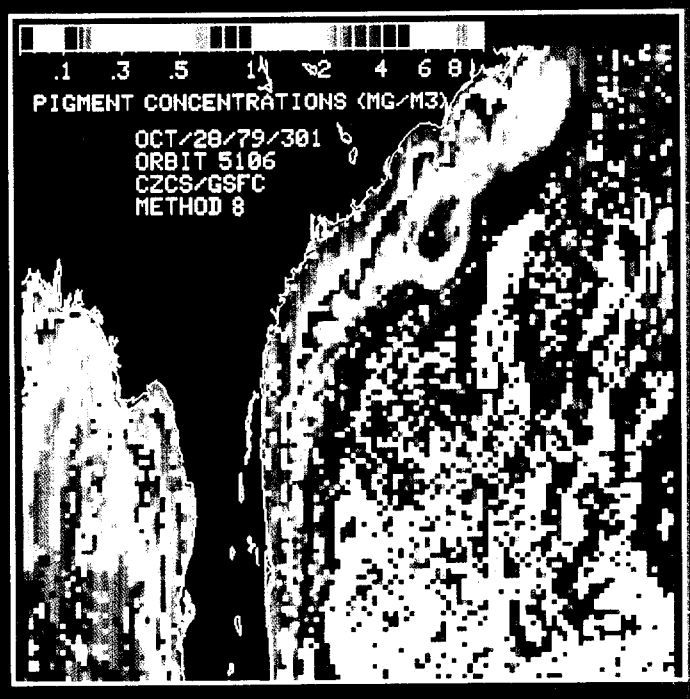

PLATE 8